A novel cost-effective choline chloride/ionic liquid solvent for all-cellulose composite production

Hester Oosthuizen[a,2], Elizabeth L du Toit[a,1], Mattheüs T Loots[a,3], Maria Atanasova[a,4], James Wesley-Smith[b,5], Stephani Crous[a], Michelle Weldhagen[a], Walter W Focke[a,6]

[a]*Institute of Applied Materials, Department of Chemical Engineering, University of Pretoria Private Bag X20, Hatfield 0028 South Africa*

[b]*Sefako Makgatho Health Sciences University, EM Unit, Molotlegi Street, Ga-Rankuwa Zone 1, Ga-Rankuwa, 0208 South Africa.*

[1] Corresponding author: elizbe.dutoit@up.ac.za; https://orcid.org/0000-0001-5579-1231

[2] u14202019@tuks.co.za; https://orcid.org/0000-0002-1296-2464

[3] theodor.loots@up.ac.za

[4] mtgster@gmail.com

[5] jameswesleysmith.smu@gmail.com

[6] walter.focke@up.ac.za; https://orcid.org/0000-0002-8512-8948

Abstract

The potential of a blended cellulose solvent, consisting of a 1:1 mass ratio of choline chloride with the ionic liquid 1-ethyl-3-methylimadazolium acetate, was evaluated by using a film-casting technique. When comparing films produced with the neat ionic liquid to casting products from the mixed solvent, mechanical properties could largely be retained, while transparency was somewhat impaired. This is attributed to a fibrous microstructure and a higher degree of crystallinity caused by incomplete dissolution of the initial cellulose fibres. The presence of these residual fibres significantly reduced shrinkage during the film formation process. Functional group analyses, together with information on their crystallographic structure, proved that these film-like products should be classified as all-cellulose composites (ACCs). Statistical analyses of tensile properties justify further research on the mixed solvent system for cellulose processing.

Keywords: cellulose solvents; 1-ethyl-3-methylimadazolium acetate; choline chloride; all-cellulose composites

Introduction

Due to their versatility, cost effectiveness and wide range of applications, plastic film production is still increasing exponentially. Unfortunately, as a consequence of their mainly single-use and mostly non-biodegradable nature, plastic films contribute to the high concentration and global distribution of plastic pollution

(Wilcox et al. 2015). Subsequently, research in biomass derived films is of great importance to academia and industry. Due to its abundance and renewable nature, cellulose has great potential to be used as a bio-degradable bio-polymer source for film production. Although cellophane and cuprophane cellulose type films are available on the market, their production and use have decreased since the 1960s following the development of synthetic polymers with superior properties. The environmental pollution associated with the generation of harmful gases such as CS_2, H_2S, and NH_3 during the traditional production of these regenerated cellulose films and fibres also hinders their widespread use (Wang et al. 2012; Yamane 2015). Further, cellulose does not dissolve in common organic solvents and subsequently remains largely underutilized due to processing limitations. This property can be attributed to the frequency and stereoregularity of hydroxyl groups on cellulose chains, that result from strong inter- and intramolecular hydrogen bonds (Swatloski et al. 2002; Rabideau et al. 2014; Zhang et al. 2014; Liu et al. 2015; Raut et al. 2015; Ren et al. 2017). A number of other cellulose solvent systems have been developed, but most are still limited by problems such as toxicity, cost, difficulty in solvent recovery, or instability during processing (Chen et al. 2009; Liu et al. 2015; Raut et al. 2015; Meng et al. 2017).

Ionic liquid solvents (ILs), have shown promise to improve the exploitability of this resource by successfully dissolving various forms of cellulose (Liu et al. 2012; Zhao et al. 2012; Reddy et al. 2014; Raut et al. 2015; Stolarska et al. 2017; Lethesh et al. 2020). ILs offer a number of distinct advantages over traditional solvents, including low volatility, the ability to be tailored to meet specific physicochemical goals, high thermal stability, outstanding solvation ability and a wide electrochemical window (Rabideau et al. 2014; Liu et al. 2015; Meenatchi et al. 2017; Reddy et al. 2017).

Unfortunately, these cellulose-dissolving ionic liquids are generally still prohibitively expensive. According to a techno-economic analysis performed by Klein-Marcuschamer et al. (2011), advances are needed to reduce IL cost and/or IL load needed for processing while maintaining a high degree of solvent recovery and recyclability. Therefore, the aim of this work was to investigate the possibility of using a more cost-effective solvent system for cellulose dissolution.

Specifically, a mixed solvent containing a 1:1 mixture by weight of the ionic liquid [EMIm][OAc] and choline chloride was considered. Choline chloride is a

substituted quaternary ammonium salt (Abbott et al. 2004) commonly used as an animal feed supplement. Unlike ILs, choline chloride is inexpensive and non-toxic. In the past, choline chloride has been used with several substances, like carboxylic acids (Florindo et al. 2014) and urea (Suopajärvi et al. 2017), to produce deep eutectic solvents (DES). Some choline chloride based DES have been used to dissolve small amounts of cellulose (Ren et al. 2016; Lynam et al. 2017). The hypothesis in this study is that mixtures of choline chloride with other ILs like [EMIm][OAc] may provide more cost-effective solvent systems – without sacrificing efficacy and recycle-ability. To explore the potential of this mixed solvent system, films prepared after dissolving α-cellulose in either neat [EMIm][OAc] or the novel 1:1 [EMIm][OAc]/choline chloride mixed solvent were compared. Dissolution temperature, - time and solvent to cellulose ratio were varied during the cellulose dissolution process. Tensile properties, visual appearance, film morphology, as well as thermal degradation behaviour were used as criteria for film comparison. Complimentary techniques were used to analyse the crystallographic structure and functional groups of the casting products in comparison to the α-cellulose source material.

Experimental

Materials

α-cellulose pulp, supplied by Sappi, was used as raw material. [EMIm][OAc] (>98%) was purchased from Proionic. Choline chloride (98 %) was supplied by Shaanxi Yuan Tai Biological Technology Co., Ltd.

Methods

Hand sheet preparation

Thin α-cellulose hand sheets were prepared from pulp using a Rapid Köthen hand sheet maker. The machine diluted, agitated and drained the pulp through a screen to form a sheet. The sheets were dried between two plates under vacuum (20 kPa_{abs}) and at 95 ºC. Each sheet, containing about 2 g dry α-cellulose, was approximately 0.16 mm thick and had a dry α-cellulose mass-to-area ratio of

41.5 g/m^2. Finally, 90 mm discs were cut from the hand sheets for dissolution and subsequent regenerated film production.

Film preparation

The dissolution temperature, solvent to cellulose ratio, and dissolution time were varied. Table 1 summarises the values of each of the three variables that were tested in different combinations. In total 15 different combinations of these parameters were used to prepare films using both the neat and mixed solvent. For each set of conditions, between 3 and 5 films were prepared.

Table 1: Different values of tested independent variables.

Solvent to cellulose ratio (g/g)	Dissolution temperature (°C)	Dissolution time (minutes)
9	80	30
14	90	75
19	105	120

The solvents, α-cellulose sheets and all glassware used were dried for 24 h at 105 °C prior to film preparation. The dried α-cellulose sheets were placed on top of the required amount of solvent – spread over the bottom of a petri dish. The petri dishes were left in an oven set at the dissolution temperature for the required dissolution time. After dissolution, the cellulose films were allowed to regenerate for 120 min in a closed chamber fitted with an air humidifier in which 100% saturation was maintained at a temperature of 22 °C and a pressure of 87 kPa (absolute humidity of approximately 19.42 g/m^3).

The regenerated films were rinsed with room temperature deionised water to remove the solvent from the films. Four rinsing stages of 10 min each, with 2.4 ml water per gram of solvent, were used. After rinsing, the films were clamped over short pieces of PVC piping and left to dry for at least 24 h under ambient conditions.

Analysis of cellulose films

Visual inspection

Films were inspected for visual differences including: opacity; extend of film shrinkage; fractures within the film; holes within the film; and observable undissolved fibres.

Tensile testing

All films that retained their structural integrity after drying were tested. For comparison purposes, the tensile strength of the untreated α-cellulose sheets was also recorded. Rectangular pieces of films (40 mm x 7 mm) were conditioned for 24 h at 25 – 30 °C at a relative humidity of 51 – 53 % prior to testing. Humidity control was achieved by using a saturated magnesium nitrate solution in a tightly sealed container. The stress-strain curves of the specimens were determined at 25 °C using a tensile tester (EZ-L from Shimadzu) with a 200 N load cell, an extension rate of 5 mm/min and a clamp distance of 20 mm. Ultimate tensile strength, elastic modulus and elongation at break were determined as prescribed by ASTM D882 (ASTM International 2018).

X-ray diffraction (XRD)

XRD spectra of an untreated α-cellulose sheet as well as the regenerated cellulose films were recorded on a Bruker D2 PHASER XRD Instrument with Cu Kα radiation (λ=1.54060). The system was equipped with a LYNXEYE_XE-T detector with up to 4.99° PSD opening. Samples were run as film fragments and were scanned from 5º to 50° 2θ at a rate of 0.02° 2θ steps per second.

Fourier transform-infrared spectroscopy (FTIR)

FTIR spectra of untreated α-cellulose sheets, as well as all the cellulose films prepared from the respective solvent systems were recorded using a PerkinElmer Spectrum 100 spectrophotometer. All the spectra were recorded in the ATR mode in the 4000 – 550 cm^{-1} region with 32 scans at a resolution of 4 cm^{-1}.

Scanning electron microscope imaging

The surface morphology of all the prepared regenerated films were visualised. All samples were sputter coated with chromium for 1 min and viewed using a Zeiss Supra 55VP. Most samples were viewed at an acceleration voltage of 2 kV, with the secondary detector. Very smooth samples were viewed at 0.5 kV with the in-lens detector in order to prevent degradation at high magnifications. Films were fractured in liquid nitrogen for internal morphology visualisation.

Thermogravimetric analysis

Thermogravimetric analyses (TGA) were performed using either a Hitachi STA7300 TGA-DTA or a SDT Q600 from TA Instruments. Approximately 18 mg of each sample was placed in an alumina pan and analysed in a N_2 atmosphere (flow rate of 100 ml/min). Samples were heated from room temperature to 950 °C at a heating rate of 10 °C/min. Thermograms were used to determine the extrapolated onset temperature of thermal degradation of the respective films using the tangent line technique on the TG curve according to ISO 11358-1 (International Organization for Standardization 2014).

Results and discussion

Films prepared from both solvent systems were ductile and could easily be folded without breaking. All films were characterized using the techniques described in the analysis section. Table 2 gives the sample names and tensile properties of the best films with tensile strength as selection criteria. The film naming convention is used to describe the cellulose dissolution conditions, i.e.: $F_{S,T,R,t}$ with S, the solvent used (P for neat [EMIm][OAc] and M the mixed solvent), T – dissolution temperature (°C), R – solvent to cellulose ratio (g/g) and t – dissolution time (min).

Table 2: Tensile properties of films with the highest recorded tensile strength values.

Sample (-)	Ultimate tensile strength (MPa)	Modulus (MPa)	Elongation at break (%)	Sample (-)	Ultimate tensile strength (MPa)	Modulus (MPa)	Elongation at break (%)
$F_{P,105,9,30}$	25.7	941	5.0	$F_{M,105,9,30}$	29.2	1510	9.2
$F_{P,105,9,120}$	48.4	2760	10	$F_{M,105,9,120}$	21.9	941	6.8
$F_{P,105,14,75}$	40.4	2020	13	$F_{M,105,14,75}$	21.2	872	9.9
$F_{P,90,14,75}$	52.9	2030	20	$F_{M,90,14,75}$	19.6	913	11

Stress-strain profiles used to determine the values in Table 2 are given in Figure S1 of the supplementary material. Tensile properties improved significantly after dissolution and regeneration when compared to the α-cellulose hand sheets (ultimate tensile strength: 4.3 MPa; modulus: 460 MPa; elongation at break: 1.7%).

Table 3 summarises some previously reported tensile properties of films prepared using other solvent systems for cellulose dissolution. Generally, the reported cellulose to solvent ratios are much smaller than the concentrations used in this

work (9 – 20 g solvent/g cellulose compared to 19 – 49 g solvent/g cellulose). The cellulose source (Parviainen et al. 2014; Wahlström and Suurnäkki 2015), solvent properties (Wahlström and Suurnäkki 2015; Weldemhret et al. 2020) and film preparation technique all play an important role in the ultimate cellulose film characteristics (Weldemhret et al. 2020). Films from the mixed IL/choline chloride solvent produced here had comparable tensile strength and modulus values to all-cellulose composites (ACCs) prepared by Duchemin et al. (2009) with MCC dissolved in LiCl/DMAc and that of Pang et al. (2014) – where cotton linters were dissolved in [AMIm][Cl]. Elongation at break values for films prepared from both solvent systems are comparable to the highest values reported in Table 3. This confirms their qualitatively observed ductile nature.

Table 3: Tensile properties of the regenerated ACCs and films prepared from different cellulosic sources and solvents found in literature.

Cellulose source (–)	Solvent (–)	Cellulose content (g solvent/ g cellulose)	Ultimate tensile strength (MPa)	Modulus (MPa)	Elongation at break (%)	Reference (–)
MCC	LiCl/DMAc	19	35.8	2570	2.75	(Duchemin et al., 2009)
Agave microfibril	[AMIm][Cl]	24	135	8150	3.2	(Reddy et al. 2014)
MCC	[AMIm][Cl]	24	135	8100	5.1	(Zhang et al., 2016)
Wood pulp	[AMIm][Cl]	24	100	5300	3.0	(Cao et al. 2010)
Cornhusk	[AMIm][Cl]	24	119	6550	4.1	(Cao et al. 2010)
Borassus	[AMIm][Cl]	49	111	6149	3.1	(Reddy et al. 2017)
Cotton linters	[AMIm][Cl]	19	~50	–	~6.7	(Pang et al. 2014)
Cotton linters	[EMIm][Cl]	19	119	–	8.8	(Pang et al. 2014)
Cotton linters	[EMIm][OAc]	19	~82	–	~7.3	(Pang et al. 2014)
Cotton linters	[BMIm][Cl]	19	~105	–	~8.5	(Pang et al. 2014)
Filter paper	[BMIm][Cl]	–	91.8	5750	3.76	(Duchemin et al., 2009)
MCC	[BMIm][Cl]	–	124	10800	2	(Duchemin et al., 2009)
Cellulose microfibre	[BMIm][Cl]	–	208	20000	9.8	(Yousefi et al. 2011)

During the tensile testing procedure, film test strips would consistently tear at the clamping sites of the tensile tester. This resulted in conservative measurements of the true ultimate tensile strength of the film material. In an attempt to extrapolate to more realistic values, and also to counter the effect of variance due to small lab

scale film preparation procedures, a statistical analysis was performed. Specifically, the extreme values of the underlying generating process were analysed, as extreme-value distributions have theoretical grounds for being well-suited for these type of problems (Coles 2001; Beirlant et al. 2004; de Haan and Ferreira 2006; Reiss and Thomas 2007). Complete data sets of films prepared with the neat [EMIm][OAc] solvent, as well as of films prepared with the mixed [EMIm][OAc]/choline chloride solvent, were analysed. In each case all of the preparation conditions were included.

Two different approaches were considered. A global fit of all the data by using a generalised extreme value distribution (GEV) (von Mises 1936; Jenkinson 1955), and a peak-over-threshold (POT) method by using the exponential distribution, for analysing only the tail behaviour. The former assumes that the data can be analysed in terms of block-maxima (i.e. summarised within an interval), while the latter assumes that a suitable threshold value in the data can be established, from which the tail is modelled separately from the body.

The cumulative distribution function (CDF) of the GEV, $(G(x))$, is given by Equation 1

$$Pr(X \leq x) = G(x) = exp\left[-\left(1 + shape \times \frac{(x - location)}{scale} \times \frac{-1}{shape}\right)\right] \quad (1)$$

for

$$1 + shape \times (x - location) > 0 \text{ and } scale > 0$$

The CDF of the generalised Pareto distribution (GPD), $F(x)$, (Pickands 1975) is given by Equation 2

$$Pr(X \leq x) = F(x) = 1 + shape \times \frac{(x - location)}{scale} \times \frac{-1}{shape} \quad (2)$$

where

$$1 + shape \times \frac{(x - location)}{scale} > 0 \text{ and } scale > 0 \text{ and } x > threshold$$

When the shape parameter is greater than zero, the Pareto distribution is obtained. The approximate relationship between the GEV and GPD distributions are noted, where the tail of the GEV may be modelled using the GPD by selecting an appropriate threshold value. The GPD may be used to model excess values over a high threshold. The exponential distribution is obtained as a limiting case.

For the neat solvent data, maximum-likelihood was used for parameter estimation, whereas generalised maximum likelihood was used for the mixed solvent data. Covariates were considered for all approaches and data combinations, but this non-stationarity was only detected for the global fits. This was done by using likelihood ratio tests sequentially, i.e. in a stepwise manner.

Both models predict higher ultimate tensile strength values than determined experimentally. The global fit did not rely on the highly subjective decision of a threshold value and allowed for non-stationarity. This model predicts (an average) tensile strength of double that of the average of all samples for both data sets respectively. When considering the GEV of the two film sample types, the model contained the experimental values, but much larger tensile strength values were predicted for the mixed solvent at the higher end of the data range. The POT model conservatively predicts tensile strength values of 1.7 – or 1.8 times that of the highest measured values when either the neat [EMIm][OAc] or the mixed [EMIm][OAc]/choline chloride data set is considered. The potential to produce cellulose films with desirable tensile properties from the mixed solvent system can therefore be confirmed. Data sets and details of the statistical analyses are provided as part of the Supplementary material.

If film transparency may be assumed to indicate the extent of cellulose dissolution, Figure 1 suggests that a higher degree of dissolution was achieved for films prepared with neat [EMIm][OAc] (a), (b), (c), and (d) compared to those prepared using a mixture of [EMIm][OAc] and choline chloride (e), (f), (g), and (h). It is noticeable that films prepared from the mixed solvent experienced less warpage after drying. These films also proved to be significantly more resistant to shrinkage. Figure 2 shows the radial shrinkage – calculated using Equation 3 – that the films listed in Table 2 experienced after regeneration and rinsing.

$$Radial\ shrinkage = \frac{radius_{hand\ sheet} - radius_{regenerated\ film}}{radius_{hand\ sheet}} \times 100 \quad (3)$$

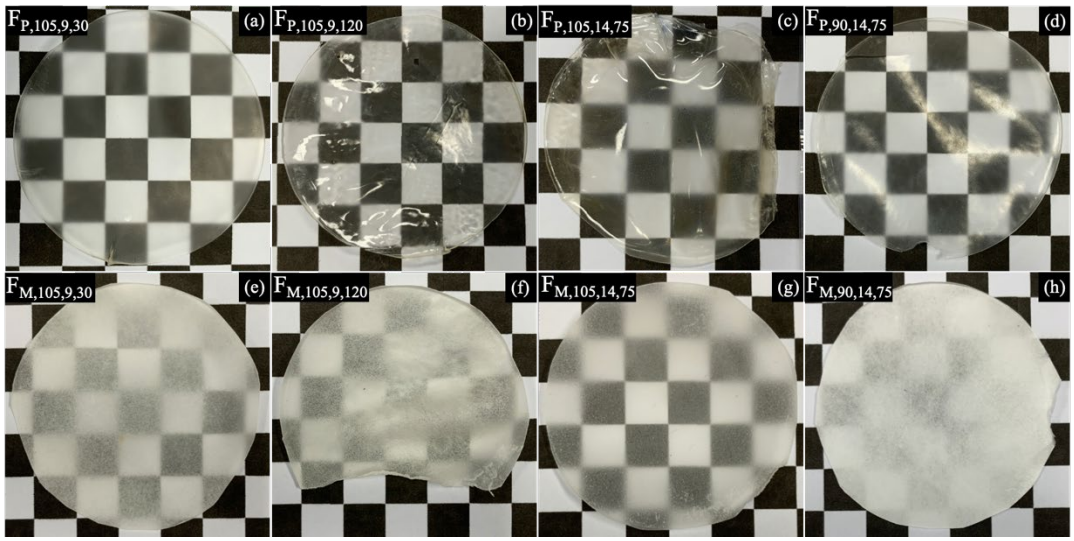

Fig. 1 Samples prepared using neat [EMIm][OAc]: (a) $F_{P,105,9,30}$, (b) $F_{P,105,9,120}$, (c) $F_{P,105,14,75}$, and (d) $F_{P,90,14,75}$ are less opaque than their counterparts prepared from the mixed solvent: (e) $F_{M,105,9,30}$, (f) $F_{M,105,9,120}$, and (g) $F_{M,105,14,75}$, and (h) $F_{M,90,14,75}$

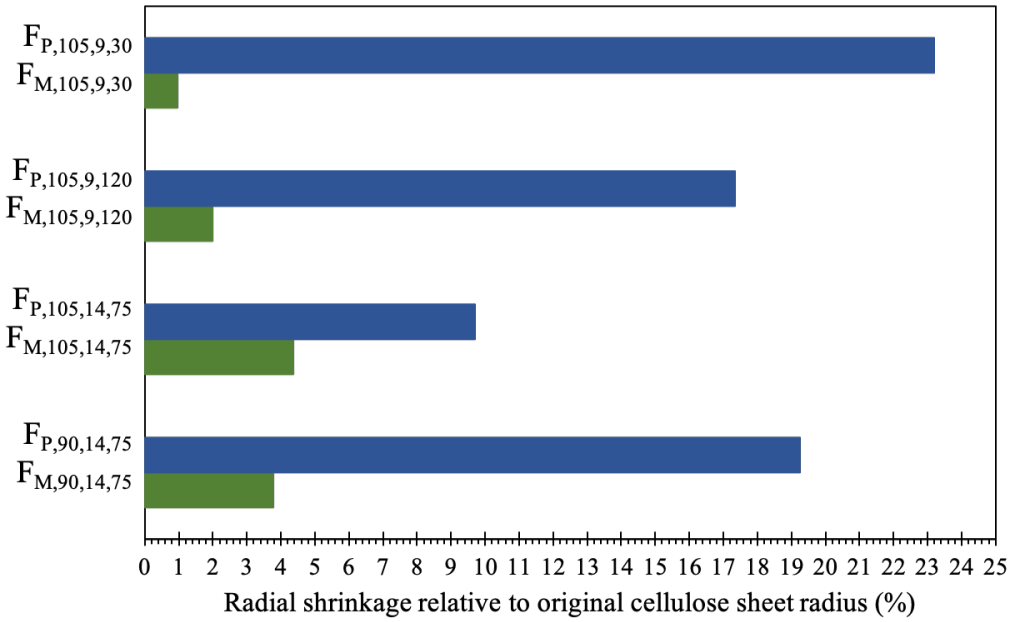

Fig. 2 Radial shrinkage of films relative to the original 90 mm α-cellulose hand sheets

In the SEM images in Figure 3 (a) – (c), the discrete nature of the cellulose fibres in the α-cellulose hand sheets before dissolution is apparent. Whereas the images of films prepared from the mixed solvent system in Figure 4, show that for these films a fused fibre surface morphology is evident.

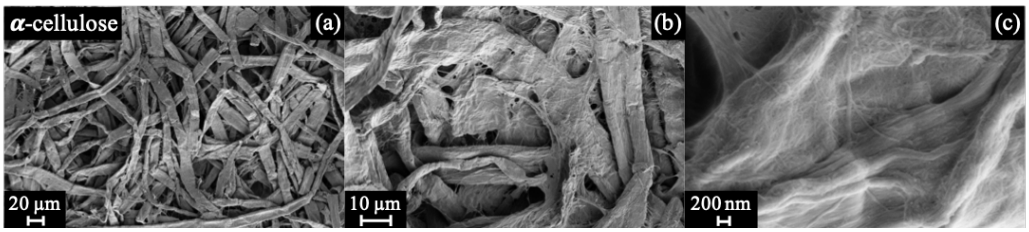

Fig. 3 SEM images of untreated α-cellulose hand sheets in order of increasing magnification

Here fibres are held together by a matrix of dissolved and regenerated cellulose. The presence of undissolved fibres in this matrix implies that these films can be classified as ACCs (Huber et al. 2012; Shibata et al. 2013). The undissolved fibres may act as reinforcement within the cellulose matrix, which can explain the resistance to warpage and shrinkage of these film types. In contrast, films prepared using neat [EMIm][OAc] exhibited a relatively smooth surface morphology – confirming a high degree of cellulose dissolution. Figure 5 gives the SEM images of these film types. The small globular structures visible at very high magnification in Figure 5 (d), (f) and (h) resemble the morphology of amorphous cellulose particles as observed by Ioelovich (2013). For both film types, images of cross sections showed that the internal structure of the films correspond with the prevalent surface morphology. For example, in Figure 6 (a) and (b) the cross sections of $F_{P,105,14,75}$ one can clearly see the smooth structure also observed on the surface of these films. Similarly, in Figure 6 (c) and (d) the fused fibre morphology observed on the surface of $F_{M,105,14,75}$ is also seen internally.

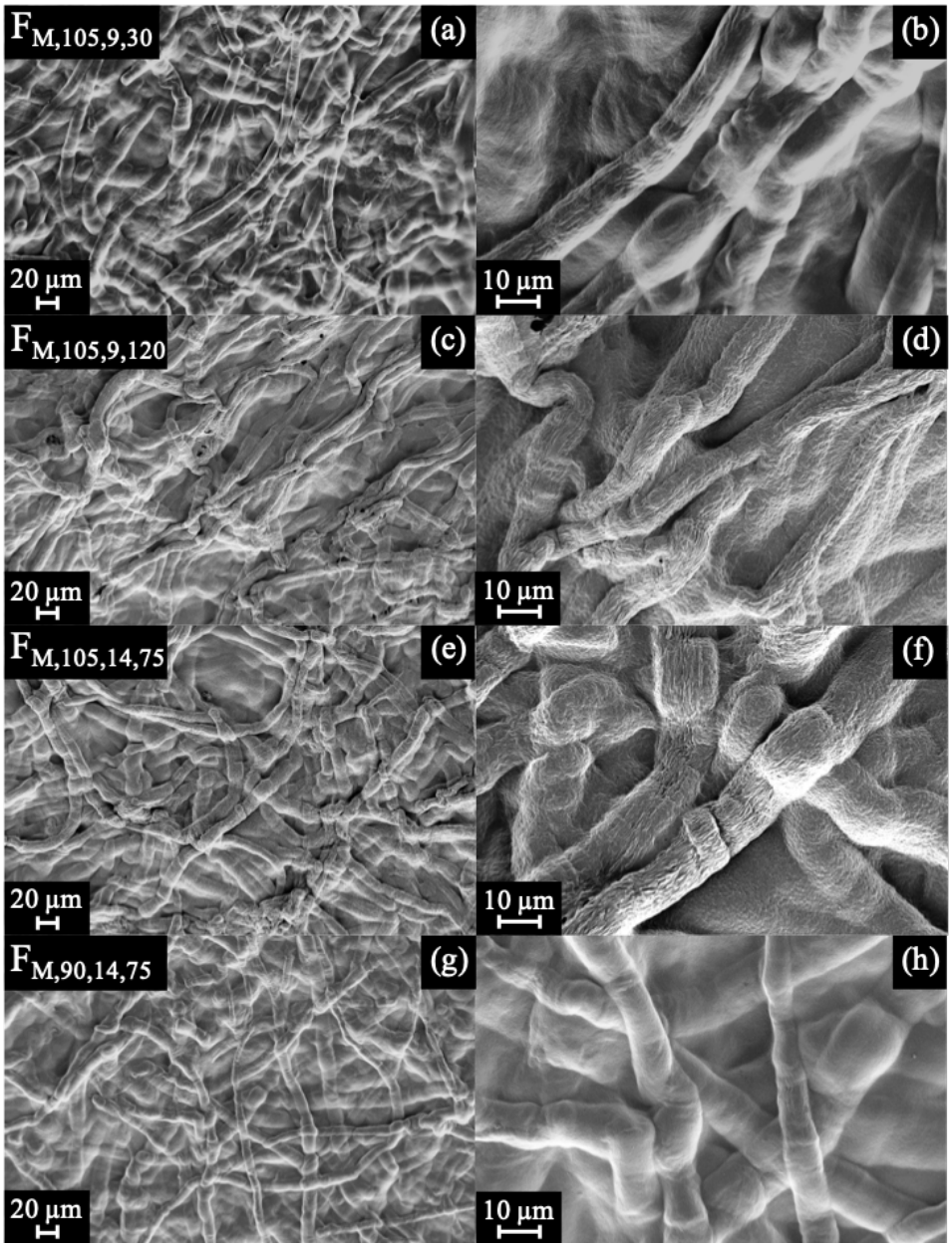

Fig. 4 SEM images of films prepared from the mixed solvent (a) and (b) $F_{M,105,9,30}$, (c) and (d) $F_{M,105,9,120}$, and (e) and (f) $F_{M,105,14,75}$, as well as (g) and (h) $F_{M,90,14,75}$ in order of increasing magnification showing the fused-fibre surface morphology of these films

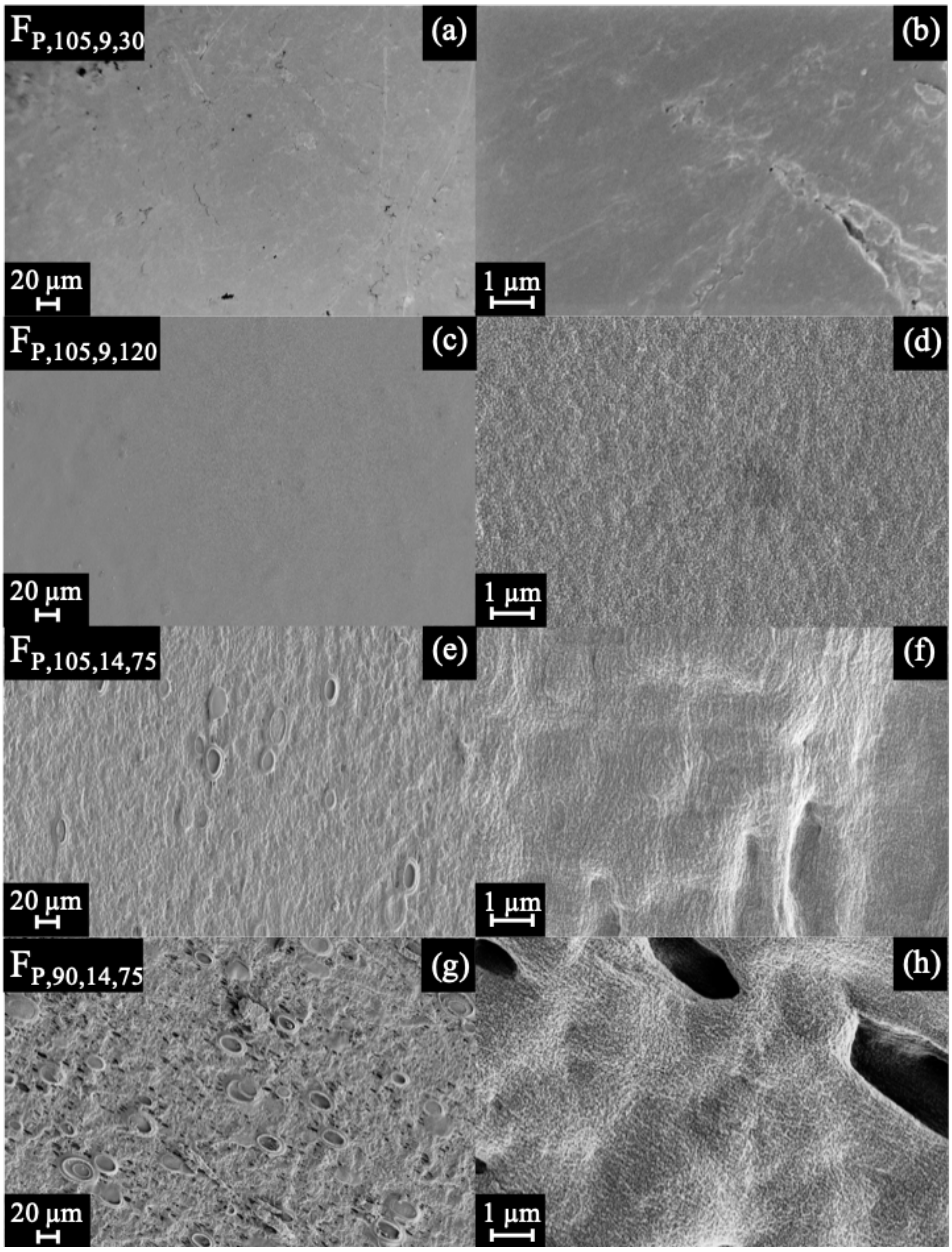

Fig. 5 SEM images of films prepared from the neat solvent: (a) and (b) $F_{P,105,9,30}$, (c) and (d) $F_{P,105,9,120}$, and (e) and (f) $F_{P,105,14,75}$, as well as (g) and (h) $F_{P,90,14,75}$ in order of increasing magnification showing the smooth surface morphology of these films

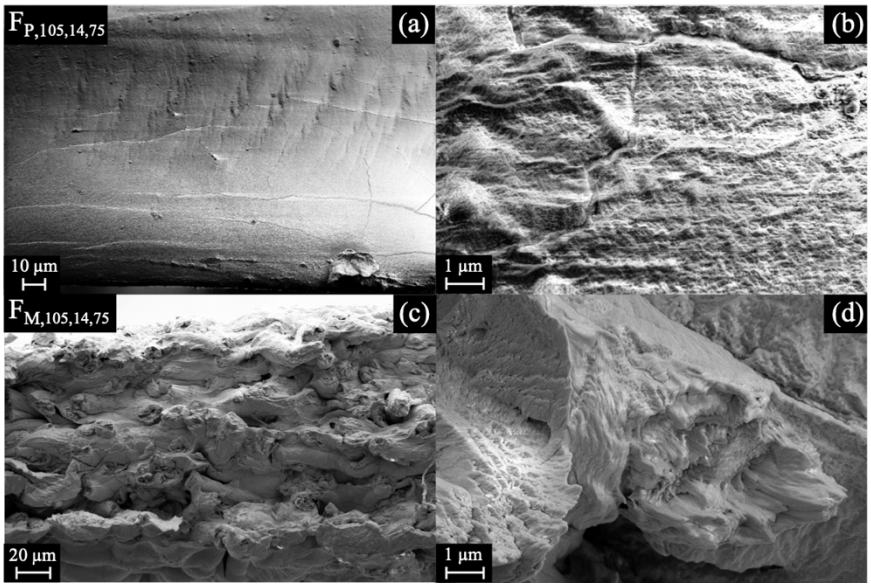

Fig. 6: SEM images showing the cross sections of selected films (a) and (b) $F_{P,105,14,75}$, and (c) and (d) $F_{M,105,14,75}$ at different magnifications illustrating the internal structure of the observed surface morphologies

In Figure 7 the XRD spectra of untreated α-cellulose hand sheets are compared to spectra of films and ACCs prepared from the respective solvent systems. These spectra support the conclusions drawn from the visual observations and SEM images. Three diffraction reflections, where 2θ is 16.7°, 22.5°, and 34.6°, are visible for the untreated α-cellulose hand sheets. These reflections correspond to the (110), (200), and (004) crystallographic planes which are characteristic of native cellulose I (Ago et al. 2004; Thygesen et al. 2005; Liu et al. 2015; Raut et al. 2015; Sun et al. 2015; Reddy et al. 2017).

In Figure 7 (a) a distinct decrease in the intensity of the spectra of films prepared with neat [EMIm][OAc] is apparent when compared to the untreated hand sheets. The distinct diffraction patterns of cellulose I disappeared. A wide reflection at around 2θ = 21.5° is visible for these films. Film $F_{P,90,14,75}$ has an additional reflection at ~12.8°, which is similar to the (1-10) characteristic secondary reflection of cellulose II at 12.1° (Ago et al. 2004). Reddy et al. (2017) attributed a similar reflection at 12.6° to cellulose II. Cellulose II has two characteristic reflections at around 20° and 22°, which corresponds to the (110) and (020) planes (French and Santiago Cintrón 2013; Reddy et al. 2017; Gong et al. 2017; Asaadi et al. 2018). With this in mind, the wide reflection exhibited by these films at 2θ = 21.7° can likely be attributed to cellulose II. The broad nature of the reflection indicates that although some cellulose II is present in these films, it is less than

amorphous cellulose (Liu et al. 2015; Reddy et al. 2017). Thus, the cellulose I structure was transformed to cellulose II and amorphous cellulose during processing, similar to other publications where cellulose dissolution was investigated (Liu et al. 2015; Raut et al. 2015; Sun et al. 2015; Reddy et al. 2017). The XRD spectra therefore confirm the amorphous nature of these films and a high degree of cellulose dissolution with the IL.

Figure 7 (b) shows the XRD spectra of films prepared with the mixed solvent. These films are more crystalline than those prepared with neat [EMIm][OAc]. In fact, their spectra still resemble that of cellulose I, but with lower intensities when compared to the untreated α-cellulose hand sheets. Characteristic reflections of the planes (004) at 2θ = 34.1°, (200) at 2θ = 22° – 22.7°, and (110) at 2θ = 15.5° – 16.9° are still clearly visible (Ago et al. 2004; Liu et al. 2015; Sun et al. 2015; Reddy et al. 2017). However, for the films prepared at 105 °C, there is an addition of a shoulder at roughly 20.8°. This could be attributed to the presence of some cellulose II, as the (110) reflection at around 20° becomes visible (French and Santiago Cintrón 2013). Further, some reflections of cellulose I and II, like (1-10) at 14.5° and (110) at 16.7° of cellulose I and (1-10) at 12.1° of cellulose II or (200) at 22.5° of cellulose I and (110) and (020) at around 20° and 22° of cellulose II, are close together. The spectra could therefore suggest the presence of cellulose I and some cellulose II as the characteristic reflections could be present as different peaks in the same area. Clearly some amorphous cellulose is present in all these films, with more amorphous material in films prepared at higher temperatures. This indicates that the novel solvent did dissolve some cellulose, transforming cellulose I to amorphous cellulose and possibly cellulose II. The presence of native cellulose in films prepared from the mixed solvent confirms that these samples can be classified as ACCs.

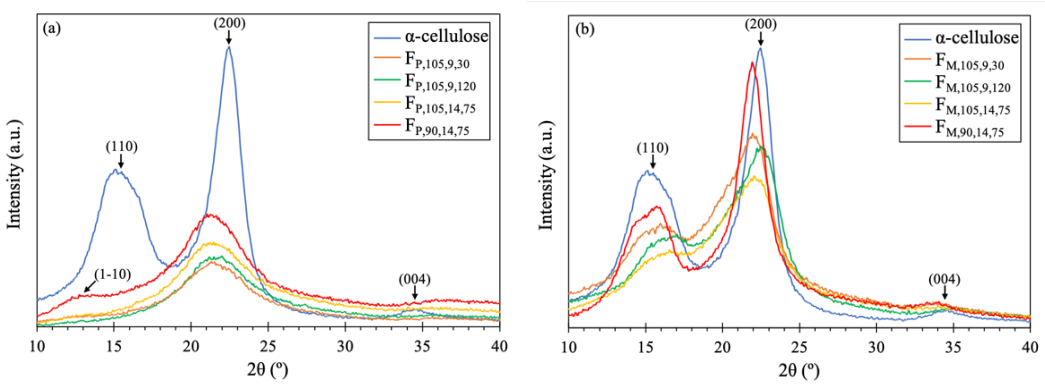

Fig. 7 XRD spectra of an untreated α-cellulose hand sheet as well as the regenerated cellulose films prepared with (a) neat [EMIm][OAc] and (b) a mixture of [EMIm][OAc] and choline chloride as solvents. Relevant conventional cellulose peak numbering is also shown (Reddy et al. 2017)

The FTIR spectra of the untreated α-cellulose hand sheets, as well as all the regenerated cellulose films, in Figure 8 (a) and (b) as well as (c) and (d), exhibit absorption bands of all major functional groups of cellulose. This includes the common absorption bands at 3336 cm^{-1} and 3278 cm^{-1} (OH stretching vibration), 2896 cm^{-1} (CH_2 stretching vibration), as well as bands at 1428 cm^{-1} (CH_2 symmetric bending of cellulose I), 1369 cm^{-1} (C-H asymmetric deformation), 1315 cm^{-1} (CH_2 wagging) and 897 cm^{-1} (β-glucosidic linkages between the sugars units) (Carrillo et al. 2004; Han et al. 2013; Pang et al. 2014; Yu et al. 2014; Liu et al. 2015; Reddy et al. 2017). As the band at 897 cm^{-1} is more pronounced in amorphous cellulose and cellulose II (Pang et al. 2014; Reddy et al. 2017), it could be attributed to a small fraction of amorphous material already present in the untreated α-cellulose sheets.

A band at around 1643 cm^{-1} (1639 – 1646 cm^{-1}) is also evident for all the samples, assigned to the bending mode of absorbed water present in the amorphous phase (Han et al. 2013; Pang et al. 2014; Reddy et al. 2017). This band increases in intensity in most of the regenerated samples, which could indicate a higher affinity for moisture after dissolution and regeneration. The relatively broader nature of the absorption band at 3000 – 3600 cm^{-1} in all the regenerated film samples compared to the spectra of the untreated α-cellulose hand sheets is indicative of the breaking of hydrogen bonds between hydroxyl groups upon dissolution (Raut et al. 2015). The absorption bands at 1428 cm^{-1}, 1369 cm^{-1}, 1160 cm^{-1}, 1105 cm^{-1} and 897 cm^{-1} can be used to investigate the type of crystalline cellulose after dissolution, as the crystalline cellulose I spectrum

differs clearly in these bands from cellulose II and amorphous cellulose (Carrillo et al. 2004; Han et al. 2013; Yu et al. 2014). When considering the FTIR spectra of films prepared with neat [EMIm][OAc] in Figure 8 (b), the absorption band detected at 1428 cm^{-1} in the neat α-cellulose hand sheet, was less intense and shifted to 1418 – 1422 cm^{-1}, characteristic for cellulose II. The cellulose I bands at 1369 cm^{-1} and 897 cm^{-1} shifted to 1367 cm^{-1} and 895 cm^{-1} associated with cellulose II (Carrillo et al. 2004; Han et al. 2013; Yu et al. 2014). The disappearance of the band at 1105 cm^{-1}, assigned as ring stretching in plane, and the increased intensity of the band at 895 cm^{-1} also indicates that the cellulose was converted into cellulose II (Han et al. 2013; Liu et al. 2015; Reddy et al. 2017). A new band at 994 cm^{-1}, which could be assigned to C-O stretching vibration in the amorphous region (Raut et al. 2015), also appears. Crystal transformation of cellulose I to cellulose II and amorphous cellulose could subsequently be assumed.

In comparison, this band at 944 cm^{-1} is much less pronounced for ACCs prepared using the mixed solvent as shown in the spectra in Figure 8 (d). In fact, a small clearly defined absorption band is only visible for $F_{M,105,14,75}$ while for the other ACCs only a shoulder is visible at 994 cm^{-1}. The shift in adsorption bands from 1428 cm^{-1}, 1369 cm^{-1}, 1160 cm^{-1} and 897 cm^{-1} for cellulose I to 1426 cm^{-1}, 1368 cm^{-1}, 1156 cm^{-1} and 896 cm^{-1} for cellulose II along with the disappearance of the band at 1105 cm^{-1} is only observed for $F_{M,105,14,75}$. No noticeable shift in absorption band positions is noticed for $F_{M,90,14,75}$ and the band at 1105 cm^{-1} is not lost. In the case of $F_{M,105,9,30}$ and $F_{M,105,9,120}$ a shift of the band from 1160 cm^{-1} to 1157 cm^{-1} is seen, and the band at 1105 cm^{-1} disappears. However, no shift of the bands at 897 cm^{-1} and 1369 cm^{-1} occurs, although the band at 897 cm^{-1} increases in intensity. This suggests that, similar to the films prepared with neat [EMIm][OAc], mainly cellulose II and amorphous cellulose could be assumed for $F_{M,105,14,75}$. In the case of $F_{M,105,9,30}$ and $F_{M,105,9,120}$ a mixture of cellulose I, cellulose II and amorphous cellulose is likely, while for $F_{M,90,14,75}$ cellulose I is still the dominant cellulose crystal structure.

An additional band present at 1565 cm^{-1} – associated with the presence of residual [EMIm][OAc] – can be observed in all spectra. For readability the FTIR spectra of [EMIm][OAc] and choline chloride are not shown, but are available in Figure S2 in the supplementary material. The use of an additional rinsing step should be

investigated in order to remove all solvent from the films. Nonetheless, the general similarity between the spectra of the regenerated films and the α-cellulose sheets confirms that [EMIm][OAc] and choline chloride act as inert, non-derivatizing solvents for cellulose.

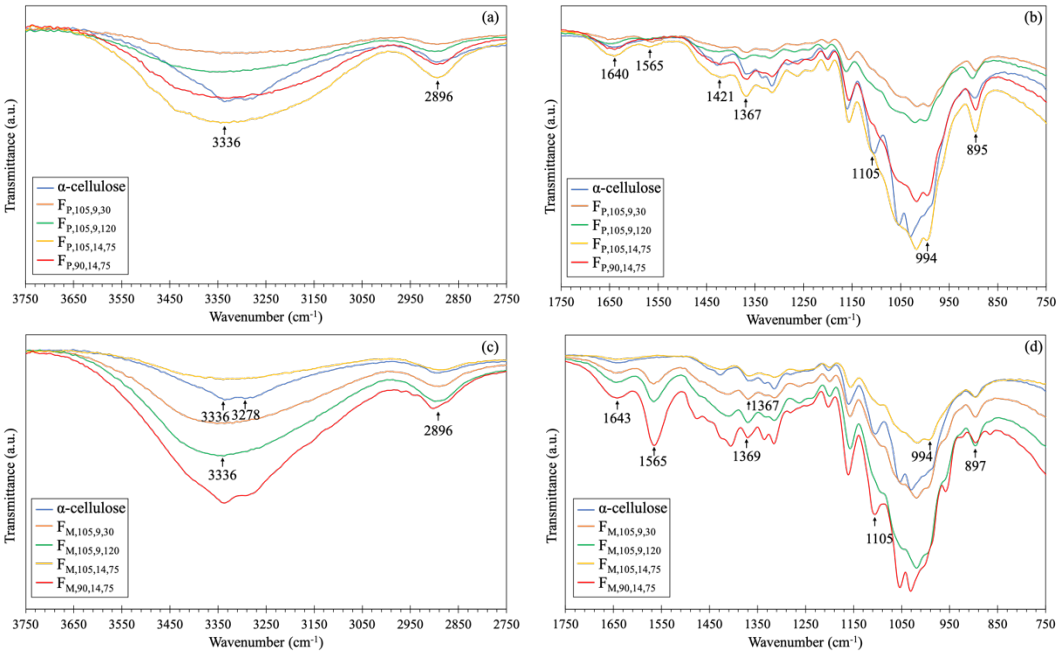

Fig. 8: FTIR transmittance spectra for films prepared with (a – b) neat [EMIm][OAc] and (c – d) the mixed solvent compared to an α-cellulose hand sheet

Table 4 summarises the calculated onset temperatures of thermal degradation (T_{onset}) of the films under consideration. A lower T_{onset} was recorded for all the regenerated films and ACCs in comparison to that of the α-cellulose hand sheets (T_{onset} = 335 °C). This is consistent with literature (Liu et al. 2012, 2015; Lethesh et al. 2016, 2020; Reddy et al. 2017) and confirms that the crystallinity of the regenerated films was reduced through dissolution and regeneration. ACCs prepared with the mixed solvent exhibited lower T_{onset} values than their counterparts prepared from the neat solvent. Hydrogen bonding between cellulose chains may be used to explain this phenomenon. According to Meenatchi et al. (2017), unmodified cellulose has a higher onset temperature of thermal degradation due to the abundance of hydrogen bonds between cellulose chains. This leads to more ordered and packed cellulose regions. The presence of residual [EMIm][OAc]/choline chloride in the matrix may disrupt some of these hydrogen bonds, resulting in a decrease in thermal stability. Recorded thermograms used to calculate the T_{onset} values reported in Table 4 are given in Figure S3 in the supplementary material.

Table 4: Average onset temperatures of thermal degradation of films from different solvent systems compared to α-cellulose hand sheets

Sample	Average T_{onset} (°C)	Sample	Average T_{onset} (°C)
$F_{P,105,9,30}$	237	$F_{M,105,9,30}$	235
$F_{P,105,9,120}$	241	$F_{M,105,9,120}$	232
$F_{P,105,14,75}$	238	$F_{M,105,14,75}$	216
$F_{P,90,14,75}$	247	$F_{M,90,14,75}$	203

Conclusions

Ductile cellulose films and ACCs were successfully prepared by means of dissolution of α-cellulose hand sheets in either neat [EMIm][OAc] or a newly proposed mixed solvent of 50 wt-% choline chloride and 50 wt-% [EMIm][OAc]. Functional group analyses using FTIR confirmed that both solvent types may be classed as non-derivatising cellulose solvents. Films produced using the mixed solvent exhibited a fused fibre morphology. The functional group analyses, complemented by the crystallographic structure inferred from XRD spectra, imply that these films may therefore be classified as ACCs. Their fibrous structure resulted in less transparent films – but they were more resistant to shrinkage and warpage during and after processing. Under selected processing conditions, films produced from the mixed solvent proved to have competitive tensile properties when compared to films prepared using the pure ionic liquid. Furthermore, statistical analyses reveal that these films have the potential to achieve an ultimate tensile strength value of 95 MPa. This is a promising result, especially when the relatively low solvent to cellulose ratios used in this work are considered. It can therefore be concluded that the choline chloride/ionic liquid mixture provides a cost-effective solvent alternative for future work on the production of biodegradable cellulose films.

References

Abbott AP, Boothby D, Capper G, Davies DL, Rasheed RK (2004) Deep Eutectic Solvents Formed between Choline Chloride and Carboxylic Acids: Versatile Alternatives to Ionic Liquids. J Am Chem Soc 126:9142–9147. https://doi.org/10.1021/ja048266j

Ago M, Endo T, Hirotsu T (2004) Crystalline transformation of native cellulose from cellulose I to cellulose ID polymorph by a ball-milling method with a specific amount of water. Cellulose 11:163–167. https://doi.org/http://dx.doi.org/10.1023/B:CELL.0000025423.32330.fa

Asaadi S, Hummel M, Ahvenainen P, Gubitosi M, Olsson U, Sixta H (2018) Structural analysis of Ioncell-F fibres from birch wood. Carbohydr Polym TA - TT - 181:893–901. https://doi.org/10.1016/j.carbpol.2017.11.062 LK - https://UnivofPretoria.on.worldcat.org/oclc/7218204508

ASTM International (2018) ASTM D882-18: Standard Test Method for Tensile Properties of Thin Plastic Sheeting,

Beirlant J, Goegebeur Y, Teugels J, Segers J (2004) Statistics of Extremes: Theory and Applicationse. Wiley, Chichester, West Sussex, England, UK

Cao Y, Li H, Zhang Y, Zhang J, He J (2010) Structure and properties of novel regenerated cellulose films prepared from cornhusk cellulose in room temperature ionic liquids. J Appl Polym Sci 116:547–554. https://doi.org/https://doi.org/10.1002/app.31273

Carrillo F, Colom X, Suñol JJ, Saurina J (2004) Structural FTIR analysis and thermal characterisation of lyocell and viscose-type fibres. Eur Polym J 40:2229–2234. https://doi.org/https://doi.org/10.1016/j.eurpolymj.2004.05.003

Chen X, Zhang Y, Cheng L, Wang H (2009) Rheology of Concentrated Cellulose Solutions in 1-Butyl-3-methylimidazolium Chloride. J Polym Environ 17:273–279. https://doi.org/10.1007/s10924-009-0149-4

Coles S (2001) An introduction to statistical modeling of extreme values. Springer-Verlag, London, UK

de Haan L, Ferreira A (2006) Extreme Value Theory: An Introduction. Springer, New York, NY, USA

Duchemin BJC, Newman RH, Staiger MP (2009) Structure–property relationship of all-cellulose composites. Compos Sci Technol 69:1225–1230. https://doi.org/https://doi.org/10.1016/j.compscitech.2009.02.027

Florindo C, Oliveira FS, Rebelo LPN, Fernandes AM, Marrucho IM (2014) Insights into the Synthesis and Properties of Deep Eutectic Solvents Based on Cholinium Chloride and Carboxylic Acids. ACS Sustain Chem Eng 2:2416–2425. https://doi.org/10.1021/sc500439w

French AD, Santiago Cintrón M (2013) Cellulose polymorphy, crystallite size, and the Segal Crystallinity Index. Cellulose 20:583–588. https://doi.org/10.1007/s10570-012-9833-y

Gong J, Li J, Xu J, Xiang Z, Mo L (2017) Research on cellulose nanocrystals produced from cellulose sources with various polymorphs. RSC Adv 7:33486–33493. https://doi.org/10.1039/C7RA06222B

Han J, Zhou C, Wu Y, Liu F, Wu Q (2013) Self-Assembling Behavior of Cellulose Nanoparticles during Freeze-Drying: Effect of Suspension Concentration, Particle Size, Crystal Structure, and Surface Charge. Biomacromolecules 14:1529–1540. https://doi.org/10.1021/bm4001734

Huber T, Müssig J, Curnow O, Pang S, Bickerton S, Staiger MP (2012) A critical review of all-cellulose composites. J Mater Sci 47:1171–1186. https://doi.org/10.1007/s10853-011-5774-3

494 International Organization for Standardization (2014) ISO 11358-1:2014(en) Plastics —
495 Thermogravimetry (TG) of polymers — Part 1: General principles

496 Ioelovich M (2013) Nanoparticles of Amorphous Cellulose and Their Properties. J Nanosci
497 Nanotechnol 1:41–45. https://doi.org/10.11648/j.nano.20130101.18

498 Jenkinson AF (1955) The frequency distribution of the annual maximum (or minimum) of
499 meteorological elements. Q J Roy Meteor Soc 81:158–171

500 Klein-Marcuschamer D, Simmons BA, Blanch HW (2011) Techno-economic analysis of a
501 lignocellulosic ethanol biorefinery with ionic liquid pre-treatment. Biofuels, Bioprod
502 Biorefining 5:562–569. https://doi.org/10.1002/bbb.303

503 Lethesh KC, Evjen S, Venkatraman V, Shah SN, Fiksdahl A (2020) Highly efficient cellulose
504 dissolution by alkaline ionic liquids. Carbohyd Polym 229:115594.
505 https://doi.org/https://doi.org/10.1016/j.carbpol.2019.115594

506 Lethesh KC, Wilfred CD, Shah SN, Uemura Y, Mutalib MIA (2016) Synthesis and
507 Characterization of Nitrile-functionalized Azepanium Ionic Liquids for the Dissolution of
508 Cellulose. Procedia Eng 148:385–391.
509 https://doi.org/https://doi.org/10.1016/j.proeng.2016.06.494

510 Liu D, Xia K, Cai W, Yang R, Wang L, Wang B (2012) Investigations about dissolution of
511 cellulose in the 1-allyl-3-alkylimidazolium chloride ionic liquids. Carbohyd Polym 87:1058–
512 1064. https://doi.org/https://doi.org/10.1016/j.carbpol.2011.08.026

513 Liu Z, Sun X, Hao M, Huang C, Xue Z, Mu T (2015) Preparation and characterization of
514 regenerated cellulose from ionic liquid using different methods. Carbohyd Polym 117:99–
515 105. https://doi.org/https://doi.org/10.1016/j.carbpol.2014.09.053

516 Lynam JG, Kumar N, Wong MJ (2017) Deep eutectic solvents' ability to solubilize lignin,
517 cellulose, and hemicellulose; thermal stability; and density. Bioresour Technol 238:684–689.
518 https://doi.org/https://doi.org/10.1016/j.biortech.2017.04.079

519 Meenatchi B, Renuga V, Manikandan A (2017) Cellulose dissolution and regeneration using
520 various imidazolium based protic ionic liquids. J Mol Liq 238:582–588.
521 https://doi.org/https://doi.org/10.1016/j.molliq.2016.05.008

522 Meng Y, Pang Z, Dong C (2017) Enhancing cellulose dissolution in ionic liquid by solid acid
523 addition. Carbohyd Polym 163:317–323.
524 https://doi.org/https://doi.org/10.1016/j.carbpol.2017.01.085

525 Pang J-H, Liu X, Wu M, Wu Y-Y, Zhang X-M, Sun R-C (2014) Fabrication and Characterization
526 of Regenerated Cellulose Films Using Different Ionic Liquids. J. Spectrosc. 1–8

527 Parviainen H, Parviainen A, Virtanen T, Kilpeläinen I, Ahvenainen P, Serimaa R, Grönqvist S,
528 Maloney T, Maunu SL (2014) Dissolution enthalpies of cellulose in ionic liquids. Carbohyd
529 Polym 113:67–76. https://doi.org/https://doi.org/10.1016/j.carbpol.2014.07.001

530 Pickands J (1975) Statistical Inference Using Extreme Order Statistics. Ann Stat 3:119–131.

https://doi.org/10.1214/aos/1176343003

Rabideau BD, Agarwal A, Ismail AE (2014) The Role of the Cation in the Solvation of Cellulose by Imidazolium-Based Ionic Liquids. J Phys Chem B 118:1621–1629. https://doi.org/10.1021/jp4115755

Raut DG, Sundman O, Su W, Virtanen P, Sugano Y, Kordas K, Mikkola J-P (2015) A morpholinium ionic liquid for cellulose dissolution. Carbohyd Polym 130:18–25. https://doi.org/https://doi.org/10.1016/j.carbpol.2015.04.032

Reddy KO, Maheswari CU, Dhlamini MS, Mothudi BM, Zhang J, Zhang J, Nagarajan R, Rajulu AV (2017) Preparation and characterization of regenerated cellulose films using borassus fruit fibers and an ionic liquid. Carbohyd Polym 160:203–211. https://doi.org/https://doi.org/10.1016/j.carbpol.2016.12.051

Reddy KO, Zhang J, Zhang J, Rajulu AV (2014) Preparation and properties of self-reinforced cellulose composite films from Agave microfibrils using an ionic liquid. Carbohyd Polym 114:537–545. https://doi.org/https://doi.org/10.1016/j.carbpol.2014.08.054

Reiss RD, Thomas M (2007) Statistical Analysis of Extreme Values: with applications to insurance, finance, hydrology and other fields., 3rd edn. Birkhäuser Basel

Ren H, Chen C, Guo S, Zhao D, Wang Q (2016) Synthesis of a Novel Allyl-Functionalized Deep Eutectic Solvent to Promote Dissolution of Cellulose. Bioresour Vol 11, No 4 11:8457 – 8469

Ren H, Wang Q, Guo S, Zhao D, Chen C (2017) The role and potential of morpholinium-based ionic liquids in dissolution of cellulose. Eur Polym J 92:204–212. https://doi.org/https://doi.org/10.1016/j.eurpolymj.2017.05.011

Shibata M, Teramoto N, Nakamura T, Saitoh Y (2013) All-cellulose and all-wood composites by partial dissolution of cotton fabric and wood in ionic liquid. Carbohyd Polym 98:1532–1539. https://doi.org/https://doi.org/10.1016/j.carbpol.2013.07.062

Stolarska O, Pawlowska-Zygarowicz A, Soto A, Rodríguez H, Smiglak M (2017) Mixtures of ionic liquids as more efficient media for cellulose dissolution. Carbohyd Polym 178:277–285. https://doi.org/https://doi.org/10.1016/j.carbpol.2017.09.025

Sun L, Chen JY, Jiang W, Lynch V (2015) Crystalline characteristics of cellulose fiber and film regenerated from ionic liquid solution. Carbohyd Polym 118:150–155. https://doi.org/https://doi.org/10.1016/j.carbpol.2014.11.008

Suopajärvi T, Sirviö JA, Liimatainen H (2017) Nanofibrillation of deep eutectic solvent-treated paper and board cellulose pulps. Carbohyd Polym 169:167–175. https://doi.org/https://doi.org/10.1016/j.carbpol.2017.04.009

Swatloski RP, Spear SK, Holbrey JD, Rogers RD (2002) Dissolution of Cellose with Ionic Liquids. J Am Chem Soc 124:4974–4975. https://doi.org/10.1021/ja025790m

Thygesen A, Oddershede J, Lilholt H, Thomsen AB, Ståhl K (2005) On the determination of

crystallinity and cellulose content in plant fibres. Cellulose 12:563. https://doi.org/10.1007/s10570-005-9001-8

von Mises R (1936) La distribution de la plus grande de n valeurs. Rev Math Union Interbalcanique 1:141–160

Wahlström RM, Suurnäkki A (2015) Enzymatic hydrolysis of lignocellulosic polysaccharides in the presence of ionic liquids. Green Chem 17:694–714. https://doi.org/10.1039/C4GC01649A

Wang H, Gurau G, Rogers RD (2012) Ionic liquid processing of cellulose. Chem Soc Rev 41:1519–1537. https://doi.org/10.1039/C2CS15311D

Weldemhret TG, Bañares AB, Ramos KRM, Lee W-K, Nisola GM, Valdehuesa KNG, Chung W-J (2020) Current advances in ionic liquid-based pre-treatment and depolymerization of macroalgal biomass. Renew Energy 152:283–299. https://doi.org/https://doi.org/10.1016/j.renene.2020.01.054

Wilcox C, Van Sebille E, Hardesty BD (2015) Threat of plastic pollution to seabirds is global, pervasive, and increasing. P Natl Acad Sci 112:11899 LP – 11904

Yamane C (2015) Structure formation of regenerated cellulose from its solution and resultant features of high wettability: A review. Nord Pulp Pap Res J 30:78–91. https://doi.org/doi:10.3183/npprj-2015-30-01-p078-091

Yousefi H, Nishino T, Faezipour M, Ebrahimi G, Shakeri A (2011) Direct Fabrication of all-Cellulose Nanocomposite from Cellulose Microfibers Using Ionic Liquid-Based Nanowelding. Biomacromolecules 12:4080–4085. https://doi.org/10.1021/bm201147a

Yu L, Lin J, Tian F, Li X, Bian F, Wang J (2014) Cellulose nanofibrils generated from jute fibers with tunable polymorphs and crystallinity. J Mater Chem A 2:6402–6411. https://doi.org/10.1039/C4TA00004H

Zhang C, Liu R, Xiang J, Kang H, Liu Z, Huang Y (2014) Dissolution Mechanism of Cellulose in N,N-Dimethylacetamide/Lithium Chloride: Revisiting through Molecular Interactions. J Phys Chem B 118:9507–9514. https://doi.org/10.1021/jp506013c

Zhang J, Luo N, Zhang X, Xu L, Wu J, Yu J, He J, Zhang J (2016) All-Cellulose Nanocomposites Reinforced with in Situ Retained Cellulose Nanocrystals during Selective Dissolution of Cellulose in an Ionic Liquid. ACS Sustain Chem Eng 4:4417–4423. https://doi.org/10.1021/acssuschemeng.6b01034

Zhao D, Li H, Zhang J, Fu L, Liu M, Fu J, Ren P (2012) Dissolution of cellulose in phosphate-based ionic liquids. Carbohyd Polym 87:1490–1494. https://doi.org/https://doi.org/10.1016/j.carbpol.2011.09.045

Statements & Declarations

Funding

Financial support from PAMSA and the Department of Science and Innovation under Grant DST/CON 0004/2019 is gratefully acknowledged. The authors also thank Sappi for supplying of α-cellulose pulp samples as well as equipment to prepare hand sheets.

Competing Interests

The authors have no relevant financial or non-financial interests to disclose.

Author Contributions

All authors contributed to the study conception and design. Material preparation, data collection and analysis were performed by Hester Oosthuizen, Elizabeth du Toit, Mattheüs T Loots, Maria Atanasova, James Wesley-Smith, Stephani Crous, and Michelle Weldhagen. The first draft of the manuscript was written by Hester Oosthuizen and Elizabeth du Toit and final editing was done by Walter Focke and Elizabeth du Toit. All authors commented on previous versions of the manuscript. All authors read and approved the final manuscript.